Study of specific features of free rise of solid spheres in a viscous fluid at moderate Reynolds numbers

Kozelkov A.S.[1,2)], Kurkin A.A.[2)], Dmitriev S.M.[2)], Tarasova N.V.[1)],

Efremov V.R.[3)], Pelinovsky E.N.[2,4)], Strelets D.Yu.[5)]

[1)] Federal State Unitary Enterprise "Russian Federal Nuclear Center – All-Russian Research Institute of Experimental Physics", 607189, Sarov, Nizhny Novgorod region, Russia
[2)] Nizhny Novgorod State Technical University n.a. R.E. Alekseev, 603950, Nizhny Novgorod, Russia
[3] Joint-stock company "Instrument Design Bureau n.a. Academician A. Shipunov", 300041, Tula, Russia.
[4)] Institute of Applied Physics of the Russian Academy of Sciences**,** 603950, Nizhny Novgorod, Russia
[5)] Moscow Aviation Institute, 125993, Moscow, Russia

Correspondence to: Andrey Kurkin (aakurkin@gmail.com)

Abstract

The paper presents results of numerical simulations of freely rising solid spheres in a viscous fluid. The diameter of spheres was 5 mm, 7 mm, 10 mm, and 20 mm, and the corresponding Reynolds numbers varies in the interval $1400 < Re < 10100$. It has been found that the free rise path varies, as the Galileo number increases. The paper describes the principal zigzag path generating mechanism, which is determined by regularly generated and freed, oppositely oriented vortex structures, which carry away the momentum and mass of fluid from a rising sphere. Quantitative characteristics are given with respect to oscillation periods of a sphere path, transverse velocity components, and accumulation of fluid mass involved in the attached vorticity. It has been found that the vortex detachment period is coincident with the half-period of oscillations. A critical mass of a fluid in the attached vorticity has been calculated, and a mechanism of changeover from zigzagging to spiraling has been suggested.

Introduction

Throughout last decades much attention has been given to the study of the motion of bubbles and hard spheres in a fluid in a gravitational field [1 – 6]. The yielded area represents a huge field for researches due to variety of modes of motion and the broadest range of change in possible characteristic parameters.

It is also important to note that by now no agreement has been reached among researchers on many issues relating to the regularity of the motion of bubble flow in general and, even, the freely rising of a single bubble [4, 7, 8]. In order to obtain a complete picture of the bubble rise, it is necessary to take into account the nonlinear interaction of many factors, such as the physical properties of the liquid and gas filling the bubble, surface tension, inertia of the surrounding fluid, medium resistance and buoyancy. All this, as well as the three-dimensional nature of the rise, make this problem practically inaccessible for both detailed experimental study and construction of theoretical models accounting all these aspects [4, 7, 8].

As for rising/falling solid spheres of a fixed shape, the picture is clearer as compared to the case of moving bubbles, because the shape of a sphere has no effect on the dynamics of its motion. Nevertheless, in spite of the simplifications there are also some disagreements among the authors of works on this subject concerning the conditions and the occurrence time of vibrations as well as the existing types of motion [5, 9 – 12].

Due to sharp growth of computing power and development of numerical methods, direct numerical modeling has become the most common research tool in recent years, while the difficulties of creating ideal conditions and performing accurate measurements in field experiments have not yet been overcome. Direct numerical simulation of the free rise of a single bubble / sphere is carried out on the basis of the solution of the Navier-Stokes equations system for a two-phase medium in 3D formulation using the surface tension model [3 – 5, 7, 8]. Numerical studies provide detailed information on the various characteristics of this process.

Paper [7] gives numerical simulation results describing the dynamics of a single air bubble rising freely in water. The behavior of rising bubbles of different diameters, from 1 mm to 10 mm, was investigated. All rising bubbles demonstrated a zigzag, or a spiral path. It has been proposed that such path of motion is related to a varying shape of a bubble and a formation of a typical unsteady vortex wake behind the bubble, which looks like two oppositely oriented vortex trunks detached, one after another, from various sides of the bubble. It is shown that the main cause of zigzagging (which is, most likely, not the single one) is that vortexes are detached in turn from the bubble surface. The mechanism of changeover from a zigzag to a spiral path is less clear and, probably, is caused by a varying bubble shape. The numerical simulation of the free rise of single solid spheres could help us to achieve a better understanding of these phenomena, because, as mentioned above, in this case the effect of a varying shape is excluded.

The study of a single solid sphere rise, initiated by the question concerning the mechanism of the appearance of the spiral trajectory of a deformable bubble, is of particular interest. A number of papers [9 – 18] are known, connected with the study of the motion of single hard spheres in liquids possessing different properties. In contrast to air bubbles at the interphase boundary, in this case the sticking condition is realized, but not the condition of equality of the shear stresses to zero. The main influence on the nature of the rise of a solid sphere is caused by such factors as buoyancy, the moment of inertia of a particle in a fluid, viscosity and "hereditary" forces.

The rise of hard spheres is characterizing by two dimensionless numbers: the Galilei number $Ga = \sqrt{|1-m^*|\,gD^3}/\nu$ (ρ_0 is density of a sphere, ρ is density of a fluid, ν is kinematic viscosity, D is diameter of a sphere, g is gravitational acceleration), acting as dimensionless inverse viscosity (the ratio between gravity and friction), and the ratio of densities of a fluid and a solid body, $m^* = \rho_0/\rho$.

In [9], based on a large number of experiments with hard spheres with different ratios (m^*, Ga), an attempt was made to generalize the results obtained from different papers, and the regimes of motion of spherical bodies and the type of vortex trail left behind the body were

determined. One of the results of this paper is a compiled map of the modes of motion of hard spheres, obtained for a large range of numbers (m^*, Ga), and samples of the corresponding characteristic traces. It follows from this that for hard spheres there can be either a rectilinear or inclined or zigzag motion. In this case, the spheres can additionally perform either periodic or "chaotic" small vibrations, and can float without oscillations.

In paper [4], the emergence of spheres that perform "chaotic" vibrations is allocated to a separate regime. It should be noted that, despite the fact that the "spiral" trajectory is sometimes mentioned in studies on the motion of hard spheres [12, 14], recent papers on this topic [4, 9] state that oscillations interpreted as spiral are small by amplitude and wavelength relative to those that occur in one plane and represent a zigzag motion.

On the mode map of motion in [9], there are little investigated areas with insufficient data. In most papers [5, 11, 17, 18], the rise of hard spheres is investigated in a certain limited range of characteristic numbers m^* and Ga. For example, in the diagram there are few points corresponding to small Reynolds numbers Re (Re < 1000) and relatively small values of m^* ($m^* \approx 0.1 \div 0.3$). The most frequently investigated regimes correspond to the characteristic numbers $1000 < \mathrm{Re} < 10000$ [12, 14], or to small Reynolds numbers, but at $m^* > 0.5$, or $m^* < 0.05$ [16, 17].

The present work has been performed to study the free rise in the field of gravity of single solid spheres having different diameters with the same characteristic mass number $m^* = 0.2$. The study is based on solving the full system of Navier–Stokes equations using a fully implicit scheme [19]. The free rise paths of spheres 5 mm, 7 mm, 10 mm and 20 mm in diameter have been examined and the regularity of how a vortex wake past a rising sphere affects its motion path has been found out. The obtained data are compared with the mode map of motion from [9]. It should be noted that some of the results correspond to the least explored area of the diagram.

In paper [10] the rise of hard spheres ($m^* = 0.5$) with small characteristic numbers Re (Ga, respectively) were carried out. The trend in changing the character of the rise of spheres with increasing Re number was described. At first the spheres float straight, then along an inclined rectilinear trajectory, and then in zigzag fashion. A similar change in the character of the emergence of spheres as the characteristic number Ga was increased was also observed in [20]. The results of this paper confirm this trend of changing the trajectory of motion as the number Re increases.

The notion of an "entrained vorticity" is used when considering a detached vortex flow (see, for example, [21]). This is a vortex wake past a sphere having the shape of a vortex ring, which elongates downstream with time being attached and at some time it is detached. The notion of an "attached mass" implies a fluid mass involved in the entrained vorticity.

The present work justifies a hypothesis of how the fluid mass attached to a sphere affects its free rise path and causes unstable motion. The behavior of the velocity field around a rising sphere is studied. A critical value of attached mass at the time, when vortexes start detaching, and at the time, when a particle begins its periodic motion is determined. Comparison between the types of motion of a solid sphere and an air bubble [7] allows making conclusions concerning the mechanism of generating a spiral trajectory of rising bubbles.

1. A physico-mathematical model and a numerical scheme

The motion of a solid sphere is stipulated by buoyancy and resistance forces, which interaction can be represented by accounting viscosity, inertia of fluid and gravity.

The direct numerical simulation is used in the present work to numerically simulate the free rise of spherical particles, which is based on solving the Navier–Stokes equation system:

$$\begin{cases} \operatorname{div}\vec{u} = 0, \\ \dfrac{\partial \rho \vec{u}}{\partial t} + \operatorname{div}(\rho \vec{u} \otimes \vec{u}) = -\nabla p + \operatorname{div}\tau + \rho \vec{g}, \end{cases} \tag{1}$$

where ρ, $\vec{u}$, p, t is density, velocity, pressure and time, respectively; $\vec{g}$ is the gravitational acceleration vector, τ is the viscous stress tensor

$$\tau_{ij} = \mu\left(2s_{ij} - \delta_{ij}\frac{2}{3}\operatorname{div}\vec{u}\right),\ s_{ij} = \frac{1}{2}\left(\frac{\partial u_i}{\partial x_j} + \frac{\partial u_j}{\partial x_i}\right),\ i, j = 1, 2, 3.$$

Here μ is laminar viscosity.

The rigid body model is used to describe the motion of a solid sphere in a liquid:

$$\sum_{i=1}^{N}\vec{F}_i = m\frac{d\vec{V}}{dt},\ \sum_{i=1}^{P}\vec{M}_i = T\frac{d\vec{\omega}}{dt} + \vec{\omega}\times T\vec{\omega}, \tag{2}$$

where m is mass of rigid body, $\vec{F}_i$ is force applying to the body, $\vec{V}$ is translation velocity, $\vec{M}_i$ is moment applying to the body, $\vec{\omega}$ is angular velocity, T is tensor of inertia moment.

This model allows for calculations with objects moving under the action of both external forces and forces determined by the liquid-body system itself. In particular, the movement of the body under the action of hydro-aerodynamic forces and the moments created by them is taken into account. The action of the force of gravity is given directly, starting from the characteristics of the solid particle: its density and volume

$$\vec{F}_{\text{gr}} = \rho_0 \vec{g} V\ .$$

Hydrodynamic forces, including the Archimedes' force, are calculated each time step using the value of fluid pressure acting on a given particle ($\vec{F}_p$) and the friction ($\vec{F}_\tau$) force

$$\vec{F} = \vec{F}_p + \vec{F}_\tau, \quad \vec{F}_p = \int p\vec{n}dS, \quad \vec{F}_\tau = \int \mu \frac{\partial u_\tau}{\partial n} dS.$$

Here $\vec{n}$ is external normal to the verge, μ is dynamical viscosity of a fluid, u_τ is tangential velocity component, V is volume of the integration cell, S is area of the verge.

The sampling of the system (1) is performed with the method of finite volumes using an arbitrarily-shaped unstructured grid; the system is solved using the fully implicit scheme [19] based on the well-known SIMPLE algorithm [22].

To simulate a moving spherical particle, we use the approach based on the application of multiple-domain grids with overlaps (the so called "Chimera" grids) [23]. The main design area is a "basic" grid, along which a separate calculation grid, surrounding the solid, moves. At each calculation step, the resulting geometric models are combined into one grid representing the original problem (Figure 1).

Integrating of equations (2) yields new coordinates of the center of gravity of the sphere and a new angle of rotation. On the basis of the obtained data, the displacement of the nodes lying on the surface of the sphere is calculated. Together with the displacement of the nodes belonging to the surface of a solid, the whole grid region is shifted to the given boundary.

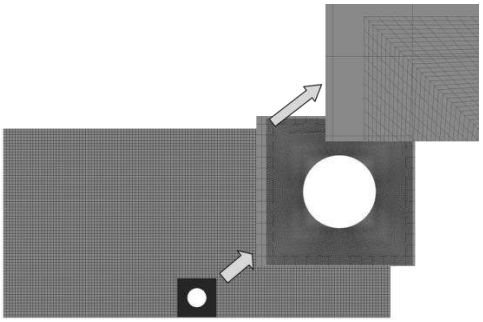

Figure 1. A computational domain with the singled out zone for a moving object

The interaction of the "base" and additional grids is realized using an interpolation template, designed for the correct interaction of topologically unconnected regions. One of the advantages of this approach is the possibility of using large enough calculation areas. The grid resolution can be coarse in regions located away from the solid, while in its vicinity a computational grid with a detailed resolution is constructed.

The described physical-mathematical model is implemented in the software package LOGOS – the software product of engineering analysis, designed to solve the conjugate three-dimensional problems of convective heat and mass transfer, aerodynamics and hydrodynamics on parallel computers [24 – 26]. Using of the multi-grid method [24] in the calculations enables

to accelerate the computational procedure significantly and to improve the efficiency of hundreds of computing cores using. The LOGOS software package has successfully passed the verification and has shown quite good results on a series of various problems including turbulent flows [26 – 28], propagation of gravitational waves on a free surface (tsunami) [19, 29, 30], industrial problems [31, 32]. All the calculations presented in this paper were carried out using the LOGOS software package.

2. Results of numerical tests

Pure water having standard properties is taken for a fluid. Spheres with $m^* = 0.2$ and diameters $D = 5, 7, 10$ and 20 mm are considered. Typical numbers for such spheres are given in Table 1.

Table 1.

Typical numbers

D, mm	5	7	10	20
Ga	1000	1640	2800	8000
Re	1400	2100	3400	10100

It should be noted that the relation between Re and *Ga* numbers taken to calculate values for this table is $\mathrm{Re} = Ga\sqrt{\frac{4}{3}\frac{1}{C_d}}$ (C_d is the drag coefficient), which in turn follows from an assumption that $F = gV(\rho - \rho_0)$ (see [9]). In our numerical tests Re numbers are calculated from the actually obtained velocity values and given below.

The calculated area is a grid with overlaps consisting of two overlapping regions: 1) a basic grid that fills the entire design area, which is a parallelepiped with dimensions 20D × 20D × 100D; 2) the grid surrounding the sphere and the filling area with the dimensions 2D × 2D × 2D, which moves along with the sphere along the basic grid. The total grid size is about 14.5 million cells. Both grids consist of hexahedrons. The characteristic cell size of the basic grid is 1.5 mm. As a result of a series of calculations on grid convergence, an optimal grid resolution was established in the vicinity of the rising sphere. The typical size of a grid cell tied to a sphere is 0.25 mm. A fragment of the grid is shown in Figure 1.

Initially, a fluid and a sphere are at rest. The boundary condition “an impenetrable wall” is set for a rising sphere. At initial time, this sphere is at a distance about one diameter to the lower

wall of the computational domain. To provide sustained computations, a time step corresponding to Courant number 0.5 is sufficient.

All results are presented in dimensionless quantities. The effective acceleration $|m^* - 1|g$ and diameter D of a sphere are used to provide zero dimension. Then, coefficients for velocity and time are $u^* = \sqrt{|m^* - 1|gD}$ and $t^* = \sqrt{\frac{D}{|m^* - 1|g}}$, respectively. The attached mass is normalized with respect to the mass of fluid forced out by the sphere, m_0.

Examination of a free rise trajectory

One of the integral quantitative characteristics of the solid sphere motion is a mean velocity of rising, which allows indirectly assessing the motion pattern. Figure 2 illustrates the time dependence of the mean velocity of rising in dimensionless quantities for spheres.

It is clearly seen from this figure that spheres of diameters 10 mm and 20 mm demonstrate that a short transient period is followed by the regime of stable oscillations and this is an evidence of periodic motion of particles. Spheres of 7 mm in diameter demonstrate weak oscillations of the free rise trajectory, which later degenerate into a straight line and this is, most likely, an evidence of the transient regime of rising, which is close to rectilinear motion. Spheres of 5 mm in diameter demonstrate no oscillations either because oscillations of the rising trajectory are insignificant, or a sphere rises rectilinearly.

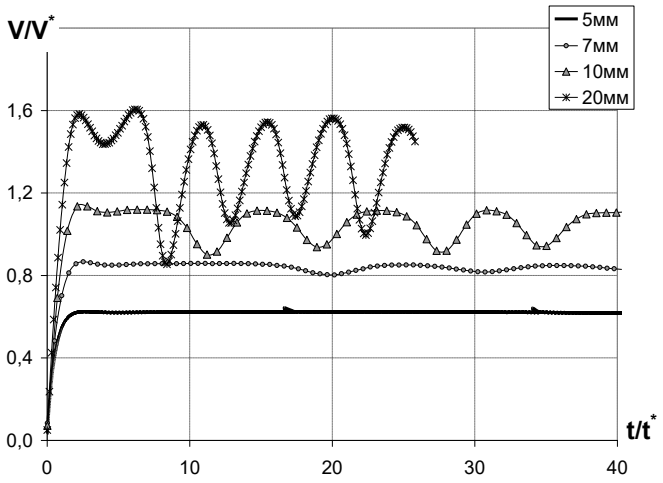

Figure 2. The free rise velocity of spheres with different diameters.

Mean values of the free rise velocity obtained in simulations correspond to Re numbers 625, 1400, 3000, and 10000. For 10 mm and 20 mm spheres, the results obtained are in a good agreement with the Re numbers from Table 1. For spheres of 5 mm and 7 mm in diameter, the

calculated velocity of rising significantly differs from the expected one and does not correspond to the map of motion regimes [9].

Figures 3-6 illustrate trajectories of spheres moving in vertical and horizontal planes.

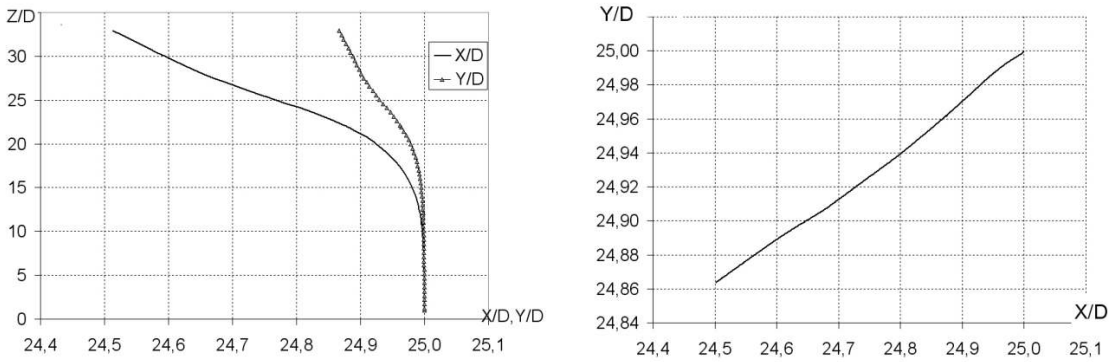

a) *b*)

Figure 3. A trajectory of moving 5 mm spheres:
a – in vertical planes (*x*-*z*) and (y-*z*); *b* – in horizontal plane (x-y).

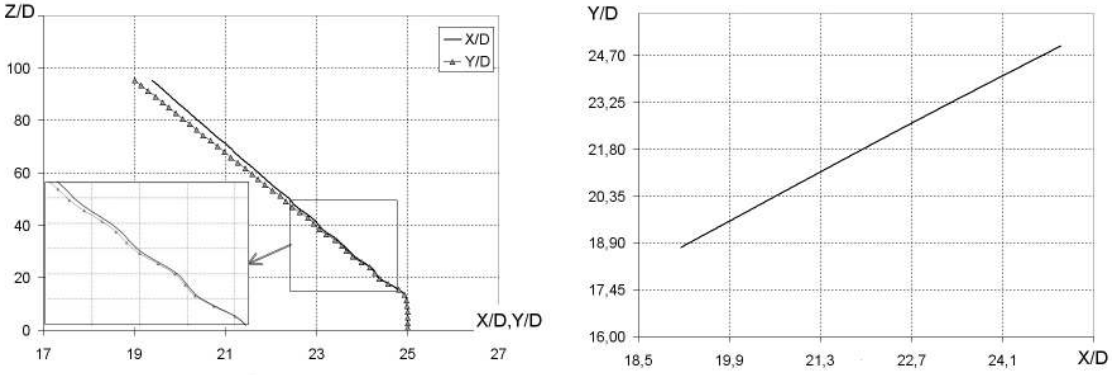

Figure 4. A trajectory of moving 7 mm spheres:
a – in vertical planes (*x*-*z*) and (y-*z*); *b* – in horizontal plane (x-y).

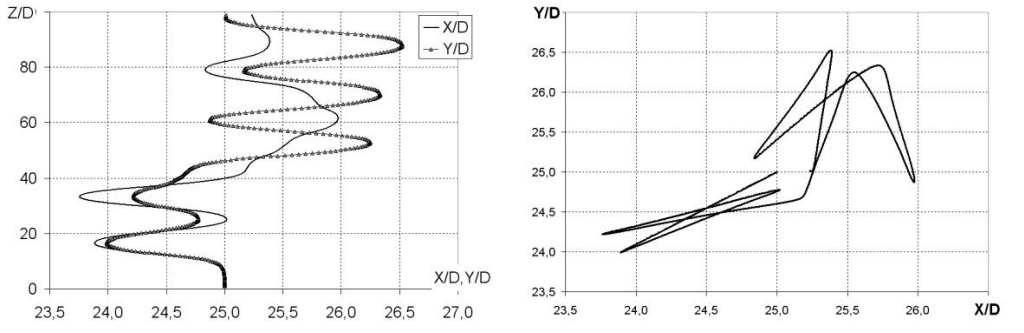

a) *b*)

Figure 5. A trajectory of moving 10 mm spheres:
a – in vertical planes (*x*-*z*) and (y-*z*); *b* – in horizontal plane (x-y).

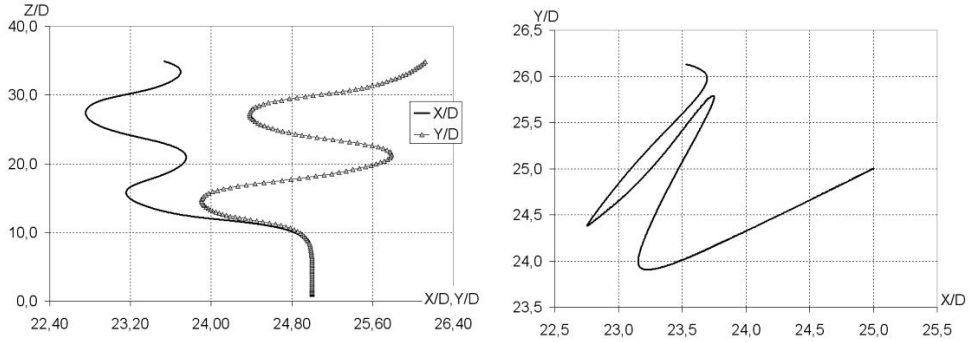

a) *b*)

Figure 6. A trajectory of moving 20 mm spheres:
a – in vertical planes (*x*-*z*) and (y-*z*); *b* – in horizontal plane (x-y)

It can be seen from these figures that 10 mm and 20 mm spheres demonstrate the periodic motion relative to both *X* axis and *Y* axis. In horizontal plane, spheres demonstrate the periodic motion, which is defined as zigzagging. It is clear from Figure 5 for 10 mm spheres that initially the zigzag motion plane is at an angle of 45 degrees to vertical coordinate planes and later it changes its position. A 20 mm sphere, upon a short stabilization period, moves in zigzags in one vertical plane.

A 7 mm sphere initially demonstrates small oscillations, then they degenerate and the free rise process continues as a rectilinear motion. Data on the trajectory of spheres 5 mm in diameter (see Figure 3) are given for the time 1s. Note that for this time horizontal displacements of such a sphere are 0.5*D*. Such motion regime should be considered rectilinear.

The conclusions concerning the behavior of moving spheres are confirmed by qualitative pictures of velocity fields in Figure 7 (vertical cuts across the center of sphere).

One can see from this figure that a vortex wake is generated behind 10 mm and 20 mm spheres, which leaves a vortex street consisting of vortexes detached one after another from various sides of a sphere. Such velocity field is an explanation to the unsteady behavior of a particle and its zigzag trajectory. For spheres of 20 mm in diameter, vortexes are more pronounced and have a higher intensity. For 5 mm and 7 mm spheres a vortex wake is symmetrical, without visible detached vortexes and this is an evidence of rectilinear motion.

Detachment of asymmetric vortexes leads to generation of the lifting force's transversal component. If a vortex is detached, the space it occupied behind the body is filled out with a fluid moving slower, the velocity decreases and the pressure increases and, hence, the side force increases. Plots of transversal velocity components for spheres of 10 mm and 20 mm in diameter given in Figure 8 illustrate these statements.

It is seen from this figure that the velocity of motion in the both transversal directions varies due to the detachment of vortexes from the body surface. Velocity fluctuations have the

same frequency and, moreover, they are synchronous and this fact also confirms that the zigzag trajectory plane is at an angle of 45 degrees to vertical coordinate planes.

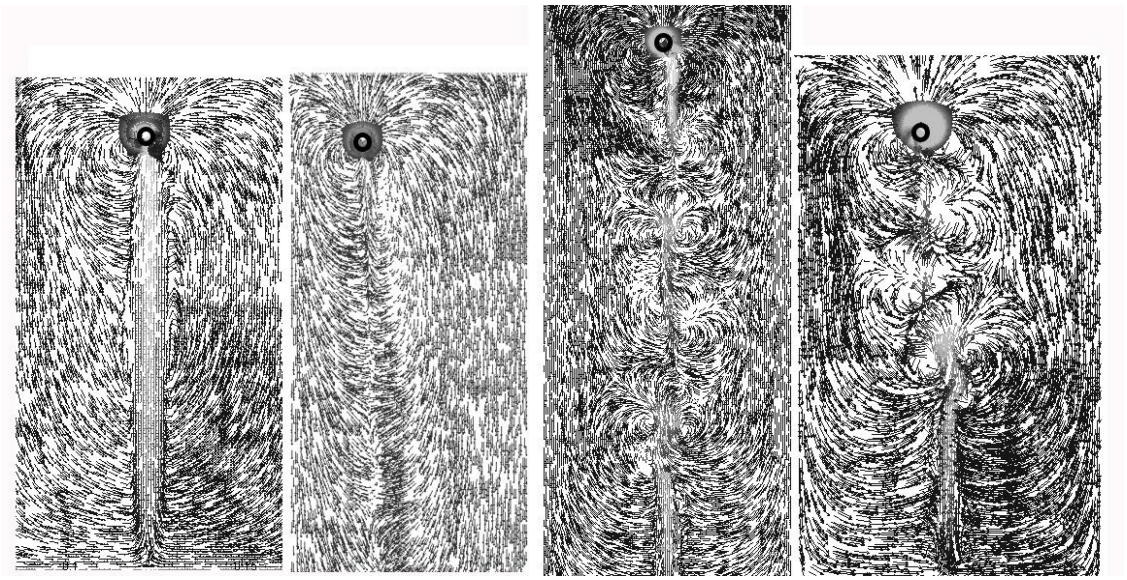

a) *b*) *c*) *d*)

Figure 7. Typical velocity fields for spheres of different diameters:
a – 5 mm; *b* – 7mm; *c* – 10 mm; *d* – 20 mm

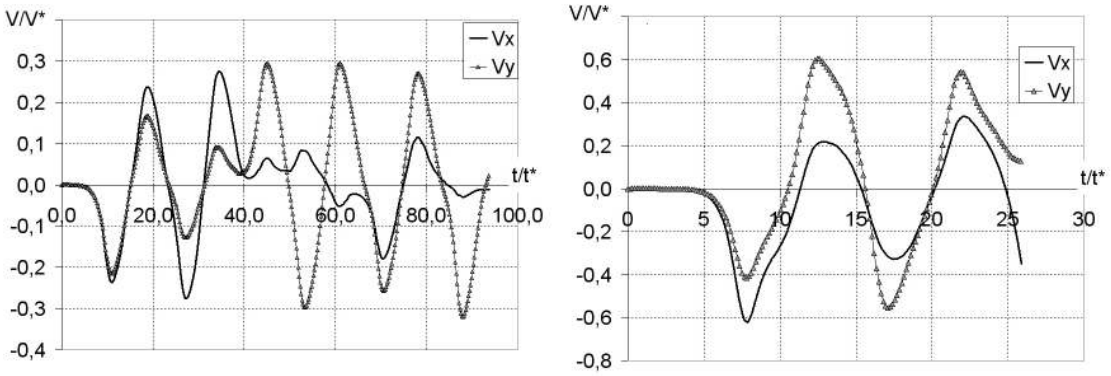

a) *b*)

Figure 8. Plots of transversal velocity components versus time:
a – *d* = 10 mm; *b* – *d* = 20 mm

Zigzagging is associated with regularly generating and freeing oppositely oriented vortex structures. Figure 9 represents typical vortex wakes for the described simulation of the motion of spheres having different diameters. They consist of double pairs of vortex trunks, which are attached to a sphere in an antisymmetric position.

It is seen that a vertically moving 5 mm sphere leaves a symmetric vortex wake without variations in the orientation of vortexes. The vortex wake past a 7 mm sphere is a chain of

vortexes with a single-side orientation owing to which a lateral lifting force is generated that promotes the inclined rise.

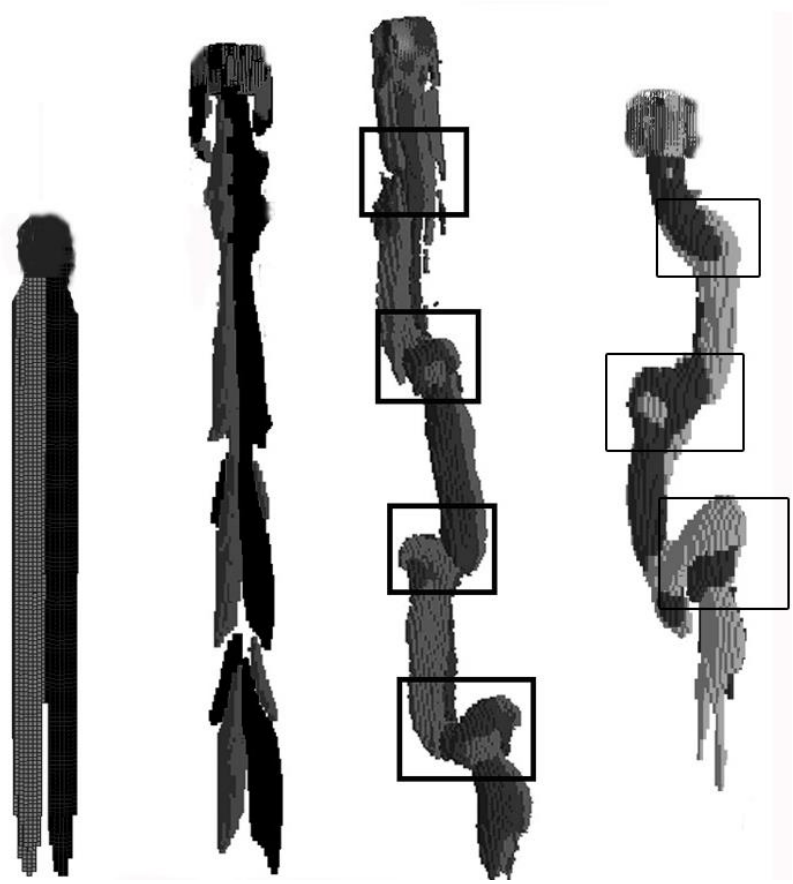

a) *b*) *c*) *d*)

Figure 9. Typical vortex wakes past moving spheres:
a – *d* = 5 mm; *b* – *d* = 7 mm; *c* – *d* = 10 mm; *d* – *d* = 20 mm

A vortex wake past spheres of 10 mm and 20 mm in diameter includes a sequence of vortex rings generated within each motion cycle of a body. With transition from one ring to another the orientation of vortexes varies. This result agrees with observations described in paper [4, 9, 13]. It [4, 9] states that vortex wakes behind zigzagging spherical particles includes four vortex rings.

Studying the attached mass effect

In this work we studied how the process of generating an attached mass affected the dynamics of vortex detachment in case of the zigzag motion.

Figure 10 graphically represents curves of the normalized attached mass versus time for spheres of diameters 10 mm and 20 mm.

These plots are periodical: at some time an accumulated attached mass achieves its critical value and this leads to its detachment from the body surface. Note that the largest mass is accumulated for the first period (when vortexes are detached for the first time). For the spheres mentioned above, a critical mass is 100 times larger than a sphere in both cases.

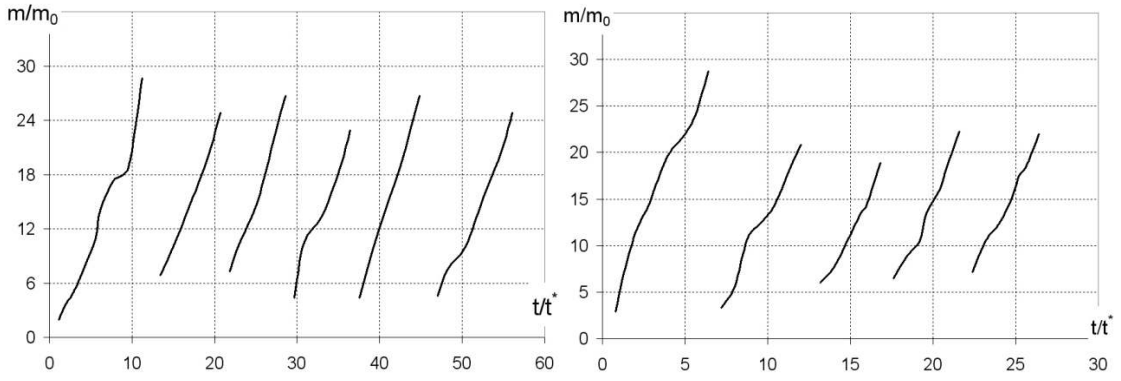

a) *b*)

Figure 10. The curves of attached mass versus time for spheres of different diameters: *a* – *d* = 10 mm; *b* – *d* = 20 mm.

The attached mass accumulation time is consistent with the vortex detachment time. Simulation data on trajectories of rising spheres (Figure 5 and 6) and curves of transversal velocity components (Figure 8) allow calculating oscillation periods for bodies and fluctuation periods for transversal velocity components, respectively. Thus, we can obtain oscillation periods from the plots of motion paths by measuring the wave motion length and dividing it by the mean free-rise velocity. It appears that the oscillation periods calculated according to the plots of transversal velocity components and motion paths are the same and equal to 16.8 s and 9.2 s for spheres with d = 10 mm and d = 20 mm, respectively. Besides, a half-period of oscillations coincides with the attached mass accumulation period. According to this data, we can assume that for one zigzag motion period vortexes are detached two times (or the attached mass comes off two times).

Conclusion

In this paper we describe the numerical study of the free rise of different-diameter solid spheres with m^* = 0.2. It has been found that the behavior of a rising sphere varies, as its diameter (or Re number) increases. A 5 mm sphere rises rectilinearly, the trajectory of a 7 mm sphere is an inclined straight line, spheres of 10 mm and 20 mm in diameter demonstrate the zigzag motion. Papers [10, 20] have already described observations of such a trend in the changeover of rising trajectory depending on an increasing Galileo number (and, hence, Re

number). The obtained data, similarly to that in [9], numerically proves the existence of rectilinear vertical motion, which was called into question in papers [10, 17].

The current study indicates that the parameters with which the rectilinear motion changes over to zigzagging need to be specified. Thus, the free rise of 10 mm and 20 mm spheres is consistent with the map of motion regimes for solid spheres in [9], while this is not true for 5 mm and 7 mm spheres. According to the diagram in [9], such spheres should move in zigzags, however, simulations demonstrate the rectilinear motion.

It follows from papers [9 – 12, 16 – 18] that the (m^*, Re) domain in the map of motion regimes, which 5 mm and 7 mm spheres fall into, is less studied. There is an insufficient numerical and experimental data for it. The critical value of mass number m^* in this domain is ~0.36 (within the range of large Re numbers Re > 1550 it approximately equals 0.6) and this indicates that, possibly, trajectories in the vicinity of critical m^* value are non-uniform. The current study suggests a hypothesis concerning the dependence of critical number m^* on Reynolds number in this domain. To confirm it, additional experimental and numerical tests are required.

Besides (see, for examples, [4, 5, 9]), to observe properly the motion in the vicinity of critical m^* values, very long stabilization time is required to avoid the effect of disturbances of various kinds..

Note that for these spheres (d = 5 mm and d = 7 mm) we have inconsistent Re numbers obtained from calculations using the mean velocity of rising and $\mathrm{Re} = Ga\sqrt{\frac{4}{3}\frac{1}{C_d}}$ formula. Possibly, the cause of such inconsistency is that the formula has been derived with an assumption of no other force acting on the given body, except the gravity and buoyant forces. In reality, the action of hydrodynamic forces on the side of fluid is a more complex process.

The present paper also shows that each of the observed free rise types demonstrates its own vortex wake. The principal mechanism of generating a zigzag trajectory is described, it is determined by regularly generated and freed vortex structures of opposite orientation, which carry away a part of the attached mass.

For zigzagging spheres, quantitative characteristics are given with respect the oscillation periods of moving sphere trajectories, transversal velocity components, and accumulation of attached masses. It has been found that the mass detachment period coincides with the half-period of oscillations of trajectories and this fact confirms the detached mass effect on the motion of particles. A critical attached mass is found to be 100 times larger than a particle mass.

Comparison of possible trajectories of rising spheres obtained in the present work and given in [9] with the results of simulations for rising air bubbles of the same diameters presented

in [7, 8] gives additional data on a possible mechanism of generating a spiral trajectory in case of bubbles. Since the spiral motion is not observed for solid spheres, there are grounds to suggest that the difference in the behavior of gas bubbles and solid spheres can be explained by the fact that bubble shapes can easily transform [4, 17]. The suggestion that the bubble shape transformation affects the changeover from zigzagging to spiraling is indirectly confirmed and a subject of further investigations. However, in spite of the difference in vortex generation mechanisms for solid spheres and bubbles the induced resistance effect on the real resistance is the same [15, 18].

Acknowledgement

This study was initiated in the framework of the state task programme in the sphere of scientific activity of the Ministry of Education and Science of Russian Federation (projects No.5.4568.2017/6.7 and No. 5.1246.2017/4.6) and with the financial support of the grants of the President of the Russian Federation for state support of leading scientific schools of the Russian Federation (NSH-2685.2018.5) and scientific researches of young Russian scientists – doctors of sciences (MD-4874.2018.9), as well as with the RFBR funding within Projects No. 16-01-00267 and No. 17-05-00067.

References

1. K. Ellingsen, F. Risso, On the rise of an ellipsoidal bubble in water: oscillatory paths and liquid induced velocity, J. Fluid. Mech. 440 (2001) 235-268.
2. C. Veldhuis, A. Biesheuvel, L. Wijngaarden, Shape oscillations on bubbles rising in clean and in tap water, Phys. fluids 20 (2008) 1-12.
3. J. Hua, J. Stene, P. Lin, Numerical simulation of 3D bubbles rising in viscous liquids using a front tracking method, J. Comp. Phys. 227 (2008) 3358-3382.
4. J.C. Cano-Lozano, C. Martinez-Bazan, J. Magnaudet, J. Tchoufag, Paths and wakes of deformable nearly spheroidal rising bubbles close to the transition to path instability, Phys. Review Fluids 1 (2016), 053604.
5. M.K. Tripathi, K.C. Sahu, R. Govindarajan, Dynamics of an initially spherical bubble rising in quiescent liquid, Nat. Commun. 6 (2015) 6268.
6. P. Ern, F. Risso, D. Fabre, J. Magnaudet, Wake-induced oscillatory paths of bodies freely rising or falling in fluids, Annu. Rev. Fluid Mech. 44 (2012) 97-121.
7. A.S. Kozelkov, A.A. Kurkin, V.V. Kurulin, S.V. Lashkin, N.V. Tarasova, E.S. Tyatyushkina, Numerical modeling of the free rise of an air bubble. Fluid Dynam. 51 (2016) 709-721.

8. H. Rusche, Computational fluid dynamics of dispersed two-phase flows at high phase fraction, Imperial College of Science, Technology & Medicine, London, 2002.
9. M. Horowitz, C.H.K. Williamson, The effect of Reynolds number on the dynamics and wakes of freely rising and falling spheres, J. Fluid Mech. 651 (2010) 251-294.
10. M. Jenny, J. Dusek, G. Bouchet, Instabilities and transition of a sphere falling or ascending freely in a Newtonian fluid, J. Fluid Mech. 508 (2004) 201-239.
11. D.G. Karamanev, The study of free rise of buoyant spheres in gas reveals the universal behaviour of free rising rigid sphere in fluid in general, Inter. J. Multiphase Flow 27 (2001) 1479-1486.
12. A.W. Preukschat, Measurements of drag coefficients for falling and rising spheres in free motion, California Institute of Technology, Pasadena, 1964.
13. M. Rahmani, A. Wachs, Free falling and rising of spherical and angular particles, Phys. Fluids 26 (2014) 083301.
14. P.B. MacCready, Y.R. Jex, Study of sphere motion and balloon wind sensors, Tech. Rep. Tech. Mem., X53089, NASA, 1964.
15. S. Krishnan, B. Sivasamy, K. Ramasamy, Transient drag coefficients from a freely rising and falling solid sphere at moderate particle Reynolds numbers, Canadian J. Chem. Eng. 94 (2016) 1003-1014.
16. M. Jenny, J. Dusek, Efficient numerical method for the direct numerical simulation of the flow past a single light moving spherical body in transitional regimes, J. Comp. Phys. 194 (2004) 215-232.
17. C.H.J. Veldhuis, A. Biesheuvel, An experimental study of the regimes of motion of spheres falling or ascending freely in a newtonian fluid, Inter. J. Multiphase Flow 33 (2007) 1074-1087.
18. C.H.J. Veldhuis, A. Biesheuvel, D. Lohse, Freely rising light solid spheres, Inter. J. Multiphase Flow 35 (2009) 312-322.
19. A.S. Kozelkov, A.A. Kurkin, E.N. Pelinovsky, E.S. Tyatyushkina, V.V. Kurulin, N.V. Tarasova, Landslide-type tsunami modelling based on the Navier-Stokes Equations, Science Tsunami Hazards 35 (2016) 106-144..
20. M. Wu, M. Gharib, Experimental studies on the shape and path of small air bubbles rising in clean water, Phys. Fluid 14 (2002) L49-L52.
21. Ph.D. Saffman, Vortex Dynamics, Cambridge University Press, Cambridge, 1992.
22. J.H. Ferziger, M. Peric, Computational methods of fluid dynamics, Springer, Berlin, 2001.
23. J.A. Benek, P.G. Buning, J.L. Steger, A 3-D Chimera Grid Embedding Technique, AIAA Paper (1985) № 85-1523.

24. K.N. Volkov, Yu.N. Deryugin, V.N. Emelianov, A.G. Karpenko, A.S. Kozelkov, I.V. Teterina, Methods for accelerating gas dynamic computations on unstructured meshes, Fizmatlit, Moscow, 2013.
25. A.S. Kozelkov, R.M. Shagaliev, V.V. Kurulin, A.V. Yalozo, S.V. Lashkin, Investigation of supercomputer capabilities for the scalable numerical simulation of computational fluid dynamics problems in industrial applications, Comput. Mathem. Mathem. Phys. 56 (2016) 1506-1516.
26. A. Kozelkov, V. Kurulin, V. Emelyanov, E. Tyatyushkina, K. Volkov, Comparison of convective flux discretization schemes in detached-eddy simulation of turbulent flows on unstructured meshes, J. Scient. Comp. 67 (2016) 176-191.
27. A.S. Kozelkov, V.V. Kurulin, Eddy resolving numerical scheme for simulation of turbulent incompressible flows, Comput. Mathem. Mathem. Phys. 55 (2015) 1255-1266.
28. A.S. Kozelkov, O.L. Krutyakova, A.A. Kurkin, V.V. Kurulin, E.S. Tyatyushkina, Zonal RANS-LES Approach Based on an Algebraic Reynolds Stress Model, Fluid Dynam. 50 (2015) 621-628.
29. A.S. Kozelkov, A.A. Kurkin, E.N. Pelinovsky, V.V. Kurulin, E.S. Tyatyushkina, Numerical modeling of the 2013 meteorite entry in Lake Chebarkul, Russia, Nat. Hazards Earth Syst. Sci. 17 (2017) 671-683.
30. A.S. Kozelkov, A.A. Kurkin, E.N. Pelinovsky, Effect of the Angle of Water Entry of a Body on the Generated Wave Heights, Fluid Dynam. 51 (2016) 288-298.
31. V.B. Betelin, R.M. Shagaliev, S.V. Aksenov, I.M. Belyakov, Yu.N. Deryuguin, A.S. Kozelkov, D.A. Korchazhkin, V.F. Nikitin, A.V. Sarazov, D.K. Zelenskiy, Mathematical simulation of hydrogen–oxygen combustion in rocket engines using LOGOS code, Acta Astronautica 96 (2014) 53-64.
32. Yu.N. Deryugin, R.N. Zhuchkov, D.K. Zelenskiy, A.S. Kozelkov, A.V. Sarazov, N.F. Kudimov, Yu.M. Lipnickiy, A.V. Panasenko, A.V. Safronov, Validation results for the LOGOS multifunction software package in solving problems of aerodynamics and gas dynamics for the lift-off and injection of launch vehicles, Mathem. Models Comp. Simul. 7 (2015) 144-153.